Received: 18 September 2018 | Revised: 4 December 2018 | Accepted: 4 January 2019

DOI: 10.1002/nbm.4068

EDITOR'S PICK

WILEY NMR IN BIOMEDICINE

Single breath-hold measurement of pulmonary gas exchange and diffusion in humans with hyperpolarized ^{129}Xe MR

Junshuai Xie[1,2] | Haidong Li[1,2] | Huiting Zhang[1] | Xiuchao Zhao[1,2] | Lei Shi[1,2] | Ming Zhang[1] | Sa Xiao[1,2] | He Deng[1,2] | Ke Wang[3] | Hao Yang[3] | Xianping Sun[1,2] | Guangyao Wu[3] | Chaohui Ye[1,2] | Xin Zhou[1,2]

[1] State Key Laboratory of Magnetic Resonance and Atomic and Molecular Physics, National Center for Magnetic Resonance in Wuhan, Wuhan Institute of Physics and Mathematics, Chinese Academy of Sciences, Wuhan, China

[2] University of Chinese Academy of Sciences, Beijing, China

[3] Department of Radiology, Zhongnan Hospital of Wuhan University, Wuhan, China

Correspondence
Xin Zhou, PhD, Professor, Wuhan Institute of Physics and Mathematics, Chinese Academy of Sciences, 30 West Xiaohongshan, Wuhan 430071, China.
Email: xinzhou@wipm.ac.cn

Funding information
Key Research Program of Frontier Sciences, CAS, Grant/Award Number: QYZDY-SSW-SLH018; National Key R&D Program of China, Grant/Award Numbers: 2016YFC1304700 and 2017YFA0505400; National Natural Science Foundation of China, Grant/Award Numbers: 81227902, 81601491 and 81625011; Hubei Provincial Natural Science Foundation of China, Grant/Award Numbers: 2017CFA013 and 2018ACA143; National Program for Support of Eminent Professionals (National Program for Support of Top-notch Young Professionals)

Pulmonary diseases usually result in changes of the blood-gas exchange function in the early stages. Gas exchange across the respiratory membrane and gas diffusion in the alveoli can be quantified using hyperpolarized ^{129}Xe MR via chemical shift saturation recovery (CSSR) and diffusion-weighted imaging (DWI), respectively. Generally, CSSR and DWI data have been collected in separate breaths in humans. Unfortunately, the lung inflation level cannot be the exactly same in different breaths, which causes fluctuations in blood-gas exchange and pulmonary microstructure. Here we combine CSSR and DWI obtained with compressed sensing, to evaluate the gas diffusion and exchange function within a single breath-hold in humans. A new parameter, namely the perfusion factor of the respiratory membrane ($SVR_{d/g}$), is proposed to evaluate the gas exchange function. Hyperpolarized ^{129}Xe MR data are compared with pulmonary function tests and computed tomography examinations in healthy young, age-matched control, and chronic obstructive pulmonary disease human cohorts. $SVR_{d/g}$ decreases as the ventilation impairment and emphysema index increase. Our results indicate that the proposed method has the potential to detect the extent of lung parenchyma destruction caused by age and pulmonary diseases, and it would be useful in the early diagnosis of pulmonary diseases in clinical practice.

KEYWORDS

compressed sensing, COPD, gas exchange, hyperpolarized ^{129}Xe, lung, pulmonary microstructure

1 | INTRODUCTION

MR with hyperpolarized (HP) noble gases can enhance the MR sensitivities of gases by over four orders of magnitude above those at thermal equilibrium. Thus, it has been widely used to study gas diffusion in alveoli and blood-gas exchange across the respiratory membrane, which constitute the essential functions of the lung.[1,2] Among the candidates for HP gas lung MR, ^{129}Xe has unique advantages because it has a long spin–lattice

Abbreviations used: ADC, apparent diffusion coefficient; AMC, age-matched control; COPD, chronic obstructive pulmonary disease; CS, compressed sensing; CSSR, chemical shift saturation recovery; CT, computed tomography; d, total septal wall thickness; D_p, mean pulmonary density; DWI, diffusion-weighted MR imaging; EI, percentage of emphysema; FEV_1, forced expiratory volume in 1 s; FRC, functional residual capacity; FVC, forced vital capacity; Hct, hematocrit; HP, hyperpolarized; L_{rms}, mean airway length; MOXE, model of xenon exchange; PFT, pulmonary function test; RBC, red blood cell; SVR, surface area-to-gas volume ratio; SVR_d, dissolved surface area-to-gas volume ratio; $SVR_{d/g}$, perfusion factor of the respiratory membrane; SVR_g, surface area-to-gas volume ratio of the pulmonary airspace; T, exchange time constant; TP, tissue/plasma; V_t, percentage of tissue volume; η, fraction of RBC xenon relative to total xenon in blood

relaxation time (T_1),[3,4] good solubility in tissue/plasma (TP) and red blood cells (RBCs), and good chemical shift sensitivity to its surrounding environment.[5]

Because of these properties, HP ^{129}Xe MR has been widely utilized in previous studies to explore pulmonary microstructure and function.[6-9] On the one hand, the pulmonary blood-gas exchange function can be quantitatively characterized by measuring the dynamics of dissolved ^{129}Xe (^{129}Xe in TP and RBC) and gaseous ^{129}Xe in the lung. Xenon transfer contrast and chemical shift saturation recovery (CSSR) are widely used methods for measuring the exchange dynamics of xenon in the lung. CSSR can directly measure the dynamic information of dissolved ^{129}Xe in both TP and RBC and obtain comprehensive information regarding gas exchange. Several theoretical models have been developed to quantify pulmonary function and microstructure by analyzing the CSSR data.[7-9] Furthermore, these models have been successfully used to assess the global physiological changes caused by pulmonary diseases, such as interstitial lung disease, chronic obstructive pulmonary disease (COPD), and radiation-induced lung injury.[10-13] On the other hand, diffusion-weighted MR imaging (DWI) is a widely used technique for estimating pulmonary microstructure, and has been applied for regional visualization in human studies.[14,15] Moreover, morphological measurements have been used to comprehensively quantify the pulmonary microstructure,[16,17] and these measurements can be used to evaluate the pulmonary microstructure changes caused by age and diseases. In summary, CSSR could be used to detect the gas exchange information across the respiratory membrane while DWI could be used to detect the gas diffusion in the alveoli. Therefore, by combining CSSR and DWI, both the gas exchange and diffusion can be obtained with HP ^{129}Xe MR, which is important for understanding pulmonary diseases comprehensively. For example, it could be used for the evaluation of the changes of the surface of the respiratory membrane, which is hard to distinguish from the changes of thickness of the respiratory membrane in the traditional clinical examination.

Generally, CSSR and DWI data are collected in separate breaths in humans due to the long acquisition time, which can be more than 15 s for either CSSR[11] or DWI acquisition.[15,17] However, the lung inflation level may vary in different breaths, which unfortunately would cause fluctuations of blood-gas exchange and pulmonary microstructure.[6,18,19] Blood-gas exchange functional changes caused by lung inflation levels have been reported in the previous study,[12] eg dissolved-to-gas xenon ratio and surface area-to-gas volume ratio (SVR). Additionally, some studies have found that the morphometric size of the human pulmonary acinus measured using HP ^{129}Xe MR was affected by the lung inflation leve.[l6,19] Accordingly, it is essential to accelerate the acquisition speed for collecting CSSR and DWI data within a single breath-hold to avoid the influence of the lung inflation level on the measured parameters associated with pulmonary structure and function. Recently, compressed sensing (CS) has been confirmed to be effective in accelerating MR acquisitions[20] and has been applied to HP gas DWI, namely, CS-DWI.[21,22] By using CS-DWI, it is possible to acquire both CSSR and DWI data using HP gases MR within a single breath-hold. Thus, the respiratory membrane and pulmonary microstructure can be assessed in the identical inflation level without ionizing radiation, which would be useful in clinical practice.

In this study, both CSSR and DWI data were collected within a single breath-hold, and two parameters, namely the perfusion factor of the respiratory membrane ($SVR_{d/g}$) and the mean airway length (L_{rms}), were used to assess the respiratory membrane and pulmonary microstructure at the identical inflation level. Additionally, pulmonary physiological parameters were used to evaluate the influences of age and pulmonary diseases on the respiratory membrane and pulmonary microstructure.

2 | EXPERIMENT

The study was approved by the Institutional Review Board (IRB). Informed consent was obtained from each subject.

2.1 | Theory

Physiological parameters were extracted by fitting CSSR data to the model of xenon exchange (MOXE),[9] and the exchange time constant (T), the normalization factor (b), the fraction of RBC xenon relative to total xenon in blood (η), the barrier-to-septal ratio (ξ/d), and the pulmonary capillary transit time (t_X) were obtained directly. The total septal wall thickness (d) could be obtained by using the following equation:

$$d = \sqrt{\pi^2 DT} \tag{1}$$

by using the diffusion coefficient for xenon in the lung tissue, $D \sim 3.3 \times 10^{-6}$ cm^2/s.[12]

The dissolved surface area-to-gas volume ratio (SVR_d) and the hematocrit (Hct) could be extracted with the following approaches, respectively:

$$SVR_d = 2b/\lambda d \tag{2}$$

$$Hct = \eta/\lambda_{RBC}/(\eta/\lambda_{RBC} + (1-\eta)/\lambda_P). \tag{3}$$

By using the average Ostwald solubility of xenon in the entire lung (λ = 0.2),[12] in the RBC (λ_{RBC} = 0.19), and in the plasma (λ_P = 0.091)[23] in Equations 2 and 3, SVR_d, Hct, and the air-blood barrier thickness (ξ) could be obtained.

The pulmonary microstructural parameters were extracted from HP noble gas DWI, and the apparent diffusion coefficient (ADC) value was calculated pixel by pixel according to

$$\mathrm{ADC} = [\ln(S_0/S)]/b_1 \tag{4}$$

where S is the signal intensity of the image pixel with diffusion-weighted factor b_1 and S_0 is the intensity of the pixel without weighting.[24]

The root mean square displacement of the particle, X_{rms}, after a diffusion time t_{exp} along a given direction was determined with the following equation[25]:

$$X_{\mathrm{rms}} = \sqrt{2\, t_{\mathrm{exp}}\, D_0} \tag{5}$$

where D_0 is the free diffusion coefficient of the particle.

A proposed modification to the q-space imaging diffusion model[26] that accounted for the short diffusion time condition (diffusion time $\Delta \approx$ diffusion gradient pulse width δ) has been shown to give improved measurements in the case of restricted diffusion. Improved measurements were also found in human lung studies.[27] The diffusion time was rewritten as[26]

$$t_{\mathrm{exp}} = \Delta + \delta. \tag{6}$$

The average root mean square displacement in the case of restricted diffusion was characterized as[26]

$$L_{\mathrm{rms}} = \sqrt{2\, t_{\mathrm{exp}}\, \mathrm{ADC}}. \tag{7}$$

It was known that the SVR = $4/L_{\mathrm{m}}$ for isotropic tissues.[28] Then, the predicted gas surface area-to-gas volume ratio of the pulmonary airspace ($\mathrm{SVR_g}$) was approximately expressed as

$$\mathrm{SVR_g} = \frac{4}{L_{\mathrm{rms}}} \tag{8}$$

where L_{rms} is the global mean value here.

$\mathrm{SVR_{d/g}}$ was defined from $\mathrm{SVR_d}$ normalized to $\mathrm{SVR_g}$ as

$$\mathrm{SVR_{d/g}} = \mathrm{SVR_d}/\mathrm{SVR_g} \tag{9}$$

where $\mathrm{SVR_d}$ was obtained by fitting the CSSR data to the MOXE and $\mathrm{SVR_g}$ was extracted according to Equation 8.

2.2 | Population

Fourteen subjects were recruited, including four younger subjects (aged 24–27) and ten older subjects (aged 55–77). Pulmonary function tests (PFTs) were performed for all subjects and graded according to the GOLD Executive Summary,[29] and the older subjects received computed tomography (CT) examinations and plethysmography. The demographic information and PFT results are summarized in Table 1. The younger subjects were normal according to the PFT results (labeled as HY subjects). Five of the older subjects were normal according to the PFT results (aged 58–74, labeled as age-matched control (AMC) subjects). Five of the older subjects were in different GOLD stages according to the PFT results (aged 55–77, labeled as COPD subjects).

2.3 | MR study procedures

All experiments were performed on a 1.5 T whole-body MRI Scanner (Avanto, Siemens, Erlangen, Germany) with a horizontal magnet using a homebuilt transmit-receive vest RF coil (17.61 MHz for ^{129}Xe). HP xenon was produced with the spin-exchange optical pumping (SEOP)[30] technique using a commercial polarizer system (verImagin Healthcare, Wuhan, China) with a freeze-out accumulation procedure in a cold finger.[13] The polarizer system was equipped with a 65 W narrowed-width laser diode array (OptiGrate, Oviedo, FL, USA) and run in the flow-through mode. A gas mixture of 1% enriched ^{129}Xe (86% ^{129}Xe isotope), 89% ^{4}He, and 10% N_2 was used in this study. After the xenon accumulation process, HP gas was thawed using hot water and extracted into a 1 L Tedlar bag, which was purged to approximately 9 Pa with a vacuum pump. The available spin polarization of xenon in the Tedlar bag was approximately 15%.

Before the MR experiments, the subject inhaled 1 L of gas mixture (5% xenon +95% N_2) from two Tedlar bags connected by a Y-tube from functional residual capacity (FRC) to calibrate the flip angle and gas ^{129}Xe center frequency.[12] Afterward, the subject inhaled 1 L of gas mixture (30% xenon +70% N_2) from FRC for the CSSR and DWI experiments.

TABLE 1 Subject demographics and PFT results

Subject	Age	Sex	BMI[a], kg/m^2	FEV_1/FVC, %	FEV_1(% pred)	GOLD state
HY1[b]	25	M	19.6	84.7	114.7	Normal
HY2	27	M	23.9	85.5	153.2	Normal
HY3	27	M	22.5	86.7	117.4	Normal
HY4	24	M	20.8	83.5	119.5	Normal
AMC1	59	M	23.5	80.7	151.9	Normal
AMC2	58	M	20.2	77.7	118.9	Normal
AMC3	70	M	18.4	78.4	158.7	Normal
AMC4	70	M	26.2	79.5	105.1	Normal
AMC5	74	F	24.1	70.4	113.9	Normal
COPD1[c]	71	M	17.4	28.7	28.3	GOLD IV
COPD2	68	M	17.3	46.3	70.9	GOLD II
COPD3	55	M	27.6	67.5	84.8	GOLD I
COPD4	77	F	18.9	67.1	102.2	GOLD I
COPD5	60	M	23.3	48.9	47.8	GOLD III

[a]BMI, body-mass index.

[b]HY subjects were young subjects with normal PFT results.

[c]COPD subjects were in different GOLD stages according to the PFT results.

2.4 | Acquisitions of the CSSR and DWI MR data

The pulse sequence for collecting the CSSR and DWI data within a single breath-hold (a total time of 10 s) is shown in Figure 1. First, CSSR data were obtained for each delay time, and then 2D multi-slice DWI data were acquired using CS. For the acquisition of CSSR data, three 1.6 ms Gaussian saturation RF pulses with a flip angle of 90° (centered at +208 ppm relative to the chemical shift of xenon gas in the alveoli) separated by gradient spoilers were used to destroy the dissolved xenon magnetization (Figure 2). After a series of variable delays that controlled how much

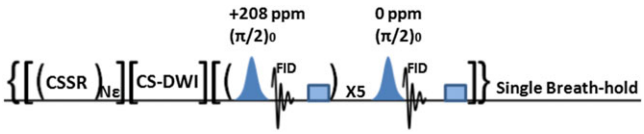

FIGURE 1 The acquisition processes of the proposed method (a total time of 10 s). First, CSSR data were obtained for different delay times with a modified sequence (a total time of 5.3 s). Then, 2D multi-slice DWI data were acquired with the CS method (CS-DWI, a total time of 4.2 s). Finally, spectra were acquired for correction of the flip angle difference between gaseous xenon and dissolved xenon (a total time of 0.4 s). *N* is the number of different blood-gas exchange delay times *ε*

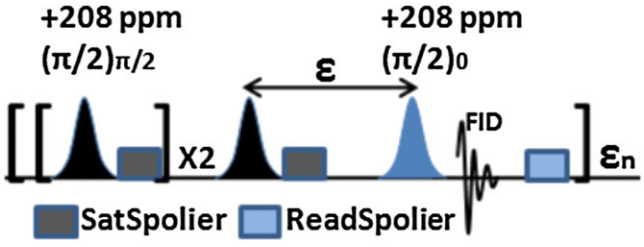

FIGURE 2 Pulse sequence diagram for the CSSR acquisition. The dissolved phase xenon magnetization was destroyed by three 1.6 ms gauss RF pulses (centered at +208 ppm relative to the chemical shift of xenon gas in the alveoli) separated by gradient spoilers. Following a variable delay time *ε*, a 1.2 ms gauss RF pulse (centered at +208 ppm) was applied and an FID was collected (bandwidth = 10 kHz, 512 data points). The process was repeated within the same breath-hold with *ε* ranging from 5 ms to 700 ms

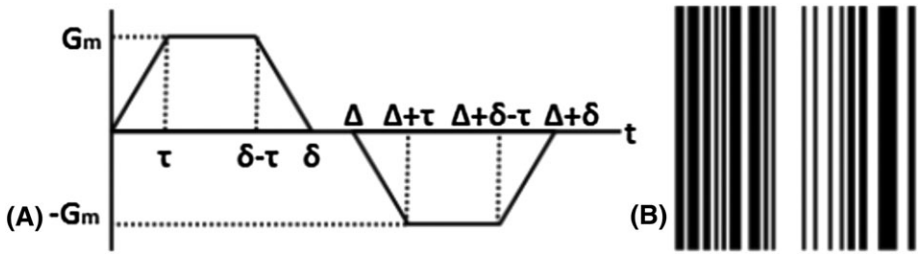

FIGURE 3 Diagram of the diffusion gradients and acquisition pattern of CS-DWI. A, diffusion-sensitizing pulse gradient waveform. Characteristic parameters of the waveform included the maximum gradient amplitude G_m, the diffusion time Δ, the pulse width δ, and the ramp time τ. B, the 2D CS undersampling pattern with a reduction factor (R) of 2. The black points are those not sampled. For human experiments, 2D diffusion-weighted HP ^{129}Xe images were acquired in a coronal plane using a multi-slice spoiled gradient recalled echo sequence (FOV = 384 × 384 mm^2, matrix size = 64 × 64, slices = 5, thickness = 25 mm, flip angle = 9°, bandwidth = 12.5 kHz, and R = 2). Diffusion weighting was achieved by using bipolar gradients (G_m = 28.395 mT/m, $\Delta = \delta$ = 3.6 ms, τ = 0.3 ms) with a b-value of 12 s/cm^2

xenon gas could enter into the lung parenchyma and the blood from the alveolar airspace, a 1.2 ms Gaussian excitation RF pulse with a flip angle of 90° (centered at +208 ppm) was applied for data collection (TE = 0.7 ms, bandwidth = 10 kHz, 512 data points). The process was repeated 21 times during the same breath-hold with a delay time ranging from 5 ms to 700 ms (a total time of 5.3 s). For the acquisition of the DWI data, 2D diffusion-weighted HP ^{129}Xe images were acquired with the CS method[23] in the coronal plane using a multi-slice spoiled gradient recalled echo sequence (FOV = 384 × 384 mm^2, matrix size = 64 × 64, slices = 5, thickness = 25 mm, flip angle = 9°, TR/TE = 13.10/9.54 ms, bandwidth = 12.5 kHz, reduction factor R = 2, total acquisition time = 4.2 s). Diffusion weighting was achieved by using bipolar gradients (amplitude = 28.395 mT/m, $\Delta = \delta$ = 3.6 ms, τ = 0.3 ms) with a b-value of 12 s/cm^2 (Figure 3). For each diffusion-weighted image, an accompanying unweighted image was acquired first in an interleaved fashion in each line of k-space. After acquiring the DWI data, spectra were acquired for correction of the flip angle difference between gaseous xenon and dissolved xenon (a total time of 0.4 s) and the process was similar to the concept in Reference 12.

2.5 | CT scans

CT was performed on a dual-energy 64-slice spiral CT scanner (Somatom Definition, Siemens). The entire lung was acquired from the apex to the bottom with subjects in supine position and in deep inspiration breath-hold before scanning. The scanning parameters were as follows: voltage, 120 kV; current, 160–180 mA s; matrix, 512 × 512; pitch, 0.75–1.0 mm; scanning layer thickness, 1 mm. Multiplanar reconstruction technology was used to observe the lung and bronchi.

2.6 | Data processing

The parameters, namely, SVR_d, d, and η, were obtained by fitting the CSSR data to the MOXE model using the nonlinear least squares method in MATLAB (MathWorks, Natick, MA, USA). The TP-to-gas ratio (TP/gas), RBC-to-gas ratio (RBC/gas), and RBC-to-TP ratio (RBC/TP) of xenon were also summarized from CSSR data with delay time 100 ms.[12] After applying a Hanning filter to the k-space data, the DWI data were reconstructed with the nonlinear conjugation algorithm.[20] The ADC of each slice and whole lung were calculated from the magnitude images after the threshold segmentation and calibration of the signal attenuation from RF excitation.[15] Then, L_{rms} and $SVR_{d/g}$ were calculated according to Equation 7 and Equation 9, respectively. CT data were analyzed using Pulmonary Toolkit (PTK)[31] to determine the percentage of emphysema (EI), mean pulmonary density (D_p), and percentage of tissue volume (V_t) on a whole lung basis.

2.7 | Statistical analysis

The parameters obtained with HP ^{129}Xe MR, PFTs, and CT (ie SVR_d, d, η, ADC, TP/gas, RBC/gas, RBC/TP, L_{rms}, SVR_g and $SVR_{d/g}$, $FEEV_1$/forced vital capacity (FVC), forced expiratory volume in 1 s (FEV_1) (%pred), EI, D_p, and V_t) were statistically analyzed among the younger and older subjects with emphysema. Statistical significance was assumed for differences between the younger and older subjects that had p-values less than 0.05 in two-tailed t-tests using MATLAB. Moreover, Pearson's correlation coefficients were also calculated in MATLAB among the HP ^{129}Xe MR, PFT, and CT results in the younger and older subjects.

3 | RESULTS

3.1 | Population and PFTs

The demographic information and relevant PFT results are shown in Table 1. There were no significant differences in the age between the AMC and COPD ($P = 1$). Meanwhile, significant differences were found both between HY and AMC ($P < 0.001$) and between HY and COPD ($P < 0.001$), as shown in Table 2. There were no significant differences in the body-mass index among the groups and no significant differences between the AMC and COPD in TLC and FRC.

3.2 | CSSR and DWI results

The statistical analysis results of HP ^{129}Xe MR, PFT, and CT data are summarized in Table 2. Comparison of DW images with $b = 0$ s/cm^2 and corresponding ADC maps of HY, AMC, and COPD are shown in Figure 4. The measured parameters related to the respiratory membrane and pulmonary microstructure were consistent with the results from previous studies, and the signal-to-noise ratio of the DW images with $b = 0$ s/cm^2 was 64 ± 13. For the ratios from CSSR data, TP/gas and RBC/gas were lower in COPD than those in AMC and HY ($P < 0.05$). However, there was no significant difference in RBC/TP between AMC and COPD ($P = 0.315$).

The SVR_d of the HY subjects (195 ± 18 cm^{-1}) was consistent with the previous studies by Chang (210 ± 50 cm^{-1})[9] and by Stewart et al (200 ± 62 cm^{-1}).[32] The SVR_d of the COPD subjects (77 ± 30 cm^{-1}) agreed with the previous studies (117 ± 60 cm^{-1}) from Stewart et al.[32] Meanwhile, the changes of ADC among HY, AMC, and COPD agreed with the findings of previous studies.[15,33]

The L_{rms} in the HY group (235 ± 4 μm) was consistent with the histology results of Weibel[34] and with the morphological measurements (253 ± 37 μm).[17] L_{rms} in the AMC (258 ± 9 μm) and COPD (303 ± 31 μm) were consistent with the previous studies (260 ± 27 μm and 320 ± 72 μm, respectively) by Paulin et al.[33] SVR_g in the HY (170 ± 3 cm^{-1}) agreed with the findings (180 ± 50 cm^{-1}) by Ouriadov et al.[17] SVR_g

TABLE 2 Statistical analysis results (mean value ± SD)

	HY	AMC	COPD	p (HY-AMC)[a]	p (HY-COPD)	p (AMC-COPD)
Age, y	25.8 ± 1.5	66.2 ± 7.2	66.2 ± 8.8	<0.001	<0.001	1
BMI, kg/m^2	21.7 ± 1.9	22.5 ± 3.1	20.9 ± 4.5	0.655	0.734	0.539
SVR_d, cm^{-1}	195.5 ± 17.9	133.3 ± 18.3	77.2 ± 30.2	<0.005	<0.001	0.010
d, μm	8.8 ± 0.9	10.6 ± 2.3	9.6 ± 1.1	0.163	0.261	0.417
η	0.48 ± 0.02	0.33 ± 0.09	0.28 ± 0.12	0.015	0.021	0.531
ADC, cm^2/s	0.038 ± 0.001	0.046 ± 0.003	0.064 ± 0.013	<0.005	0.011	0.034
L_{rms}, mm	0.235 ± 0.004	0.258 ± 0.009	0.303 ± 0.031	<0.005	0.008	0.029
SVR_g, cm^{-1}	170.3 ± 2.7	155.4 ± 5.2	133.2 ± 13.9	<0.005	<0.005	0.012
$SVR_{d/g}$	1.15 ± 0.11	0.86 ± 0.09	0.57 ± 0.16	0.006	<0.001	0.013
TP/gas, %	0.94 ± 0.17	0.89 ± 0.09	0.58 ± 0.12	0.596	0.016	<0.005
RBC/gas, %	0.44 ± 0.10	0.26 ± 0.10	0.13 ± 0.03	0.038	0.007	0.036
RBC/TP	0.47 ± 0.06	0.30 ± 0.11	0.24 ± 0.06	0.022	<0.001	0.315
FEV_1/FVC, %	85.1 ± 1.3	77.4 ± 4.1	51.7 ± 16.2	0.010	0.010	0.022
FEV_1, %pred	126.3 ± 18.1	129.7 ± 24.0	66.8 ± 29.3	0.812	0.008	0.006
FRC, L	–	3.54 ± 0.24	3.45 ± 0.62	–	–	0.774
TLC, L	–	5.76 ± 0.12	5.63 ± 0.44	–	–	0.538
EI, %[b]	–	0.46 ± 0.35	13.40 ± 9.80	–	–	0.042
D_p, g/mL[b]	–	0.18 ± 0.01	0.14 ± 0.03	–	–	0.018
V_t, %[b]	–	17.8 ± 1.0	13.7 ± 2.5	–	–	0.018
SNR($b = 0$)[c]	58.7 ± 4.9	62.3 ± 14.1	69.9 ± 15.2	–	–	–

[a]Two-tailed t-tests.

[b]These were calculated from CT results in AMC and COPD subjects.

[c]Signal-to-noise ratio of the DW unweighted images.

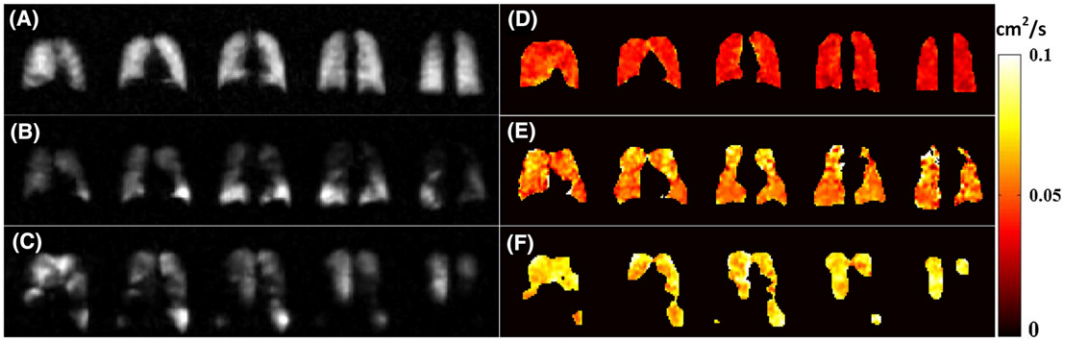

FIGURE 4 A-C, comparison of DW images with b = 0 s/cm^2 of a younger subject (group HY) (A), an older subject with normal PFT results (group AMC) (B), and a COPD subject (group COPD) (C). D-F, corresponding ADC maps

in the AMC (155 ± 5 cm^{-1}) and COPD (133 ± 14 cm^{-1}) was also consistent with the previous studies: References 18 (160 ± 50 cm^{-1} and 100 ± 40 cm^{-1}, respectively) and 33 (150 ± 16 cm^{-1} and 130 ± 28 cm^{-1}, respectively).

3.3 | Statistical analysis results among MR, PFT, and CT data

Compared with HY, the SVR_d, SVR_g, η, $SVR_{d/g}$, and FEV_1/FVC of AMC and COPD were less ($P < 0.05$) while L_{rms} was greater ($P < 0.05$). The d values of AMC (10.6 ± 2.3 μm) and COPD (9.6 ± 1.1 μm) were slightly greater ($P = 0.163$ and $P = 0.261$, respectively) than for HY (8.8 ± 0.9 μm). Compared to AMC, the SVR_d, SVR_g, $SVR_{d/g}$, D_p, and V_t of COPD were lower ($P < 0.05$) while L_{rms} and EI were higher ($P < 0.05$). However, there were no significant differences in the η and d between AMC and COPD.

For HY and AMC, SVR_d, SVR_g, $SVR_{d/g}$, and η showed a decreasing trend as age increased ($P < 0.05$), while L_{rms} showed an increasing trend as age increased ($P < 0.05$), as shown in Figure 5.

For all subjects, SVR_d, SVR_g and $SVR_{d/g}$ decreased as FEV_1/FVC ($|r| > 0.86$, $P < 0.001$) and FEV_1(%pred) ($|r| > 0.77$, $P < 0.005$) decreased, while L_{rms} correlated well with FEV_1/FVC ($r = -0.924$, $P < 0.001$) and FEV_1(%pred) ($r = -0.782$, $P < 0.001$), as shown in Figure 6.

For AMC and COPD, D_p and V_t decreased as FEV_1/FVC ($|r| > 0.96$, $P < 0.001$) and FEV_1(%pred) ($|r| > 0.91$, $P < 0.001$) decreased, while EI increased as FEV_1/FVC decreased ($r = -0.94$, $P < 0.001$) and FEV_1(%pred) decreased ($r = -0.88$, $P < 0.001$), as shown in Figure 7. Moreover, in AMC and COPD, the SVR_d, SVR_g, and $SVR_{d/g}$ decreased as EI increased ($|r| > 0.89$, $P < 0.001$) and D_p and V_t decreased ($|r| > 0.92$, $P < 0.001$), while L_{rms} correlated well with EI ($r = 0.893$, $P < 0.001$), D_p ($r = -0.92$, $P < 0.001$) and V_t ($r = -0.919$, $P < 0.001$), as shown in Figure 8.

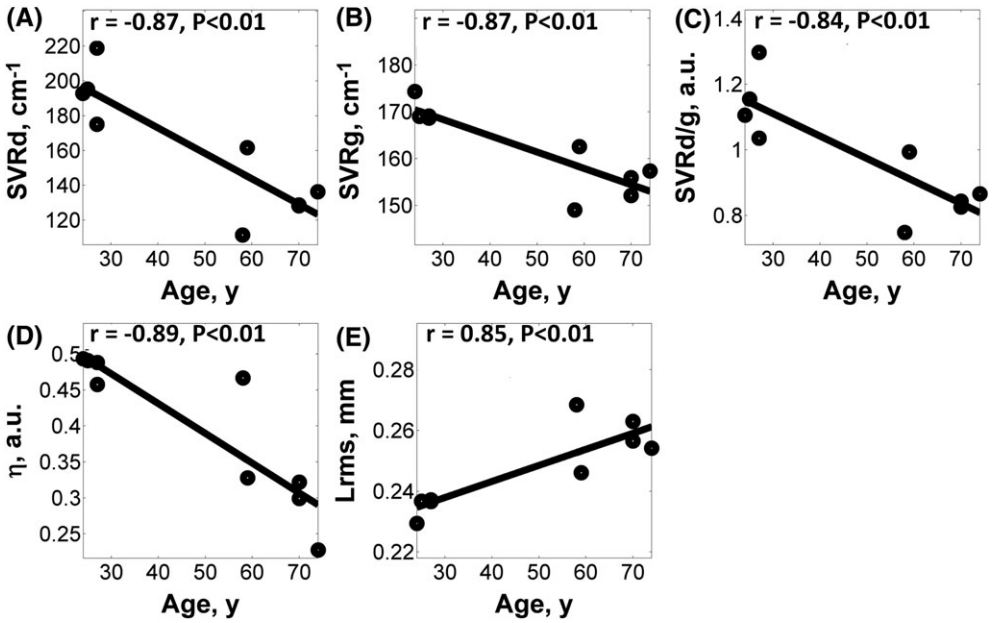

FIGURE 5 Comparison of SVR_d, SVR_g, $SVR_{d/g}$, L_{rms}, and η versus age in the HY and AMC subjects. SVR_d, SVR_g, $SVR_{d/g}$, and η showed a decreasing trend as age increased ($P < 0.05$) while L_{rms} showed an increasing trend as age increased ($P < 0.05$)

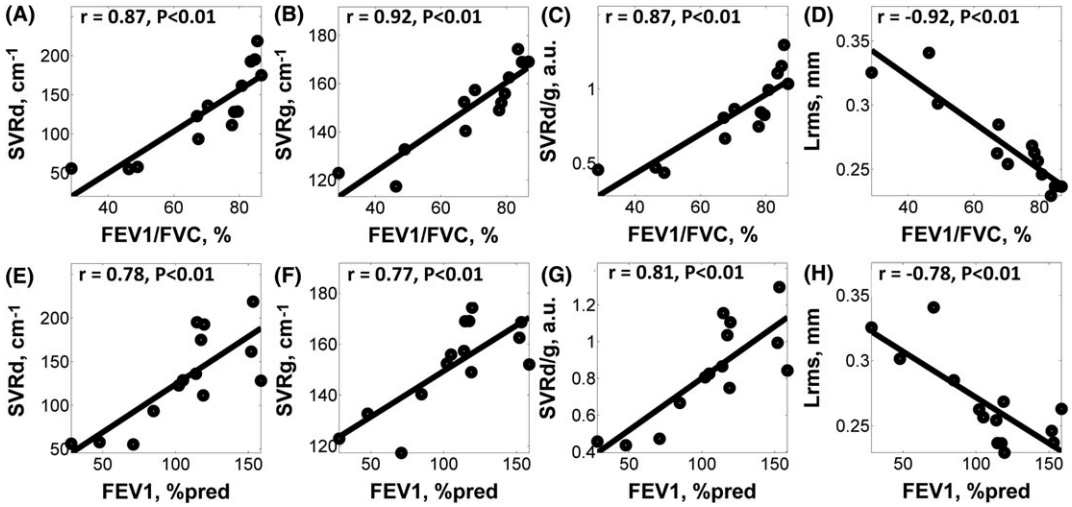

FIGURE 6 Comparison of SVR_d, SVR_g, $SVR_{d/g}$, and L_{rms} versus PFT results among all the subjects. The SVR_d (A, E), SVR_g (B, F), and $SVR_{d/g}$ (C, G) decreased as FEV_1/FVC ($|r| > 0.86$, $P < 0.01$) and FEV_1(%pred) ($|r| > 0.77$, $P < 0.01$) decreased, while L_{rms} (D, H) correlated well with FEV_1/FVC ($r = -0.924$, $P < 0.001$) and FEV_1(%pred) ($r = -0.782$, $P < 0.001$)

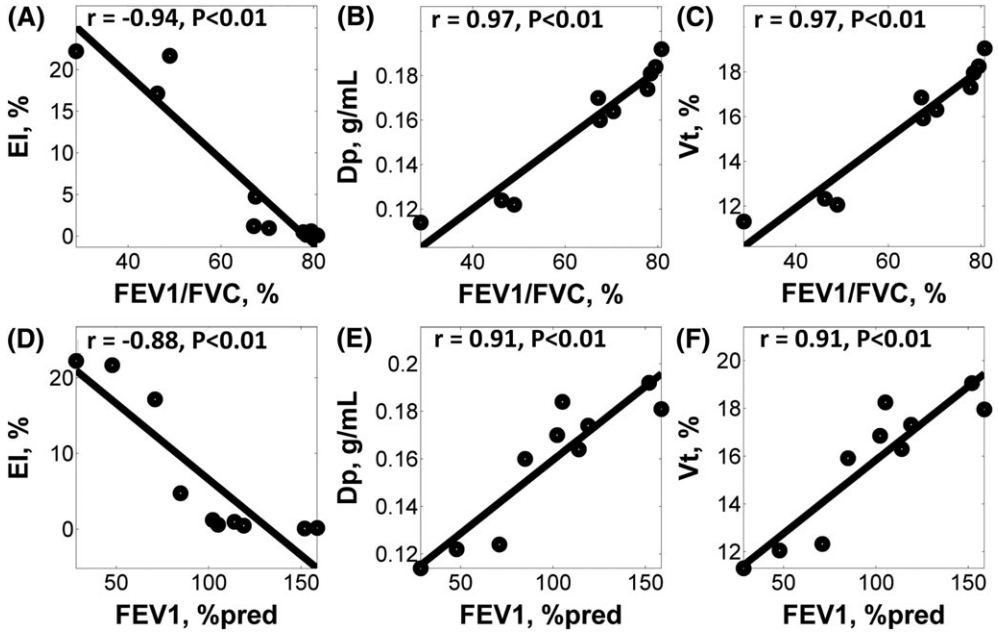

FIGURE 7 Comparison of CT versus PFT results in the AMC and COPD subjects. D_p (B, E) and V_t (C, F) decreased as FEV_1/FVC ($|r| > 0.96$, $P < 0.01$) and FEV_1(%pred) ($|r| > 0.91$, $P < 0.01$) decreased, while EI (A, D) increased as FEV_1/FVC decreased ($r = -0.94$, $P < 0.01$) and FEV_1(%pred) decreased ($r = -0.88$, $P < 0.01$)

4 | DISCUSSION

In this study, the respiratory membrane and pulmonary microstructure of humans were evaluated at identical inflation levels. The parameter, namely the perfusion factor of the respiratory membrane ($SVR_{d/g}$), was proposed to evaluate the respiratory membrane, and the parameters showed significant differences among the healthy young, AMC, and COPD subjects.

It was found that L_{rms} could be used to distinguish the older subjects from the healthy young subjects. L_{rms} was used to characterize the mean airway length in previous studies. It should be noted that L_{rms} is not the same as the mean linear intercept L_m.[16] The measured L_{rms} correlated well with age ($r = 0.854$, $P < 0.005$), which was consistent with the results of the previous study using HP gas MRI.[17,35] A recent study on explanted lungs showed that HP ^{129}Xe DWI could quantify the severity of lung parenchyma destruction, and the results correlated well with those using quantitative histology.[35] These results indicate that L_{rms} has potential to evaluate the changes of pulmonary airspace caused by age.

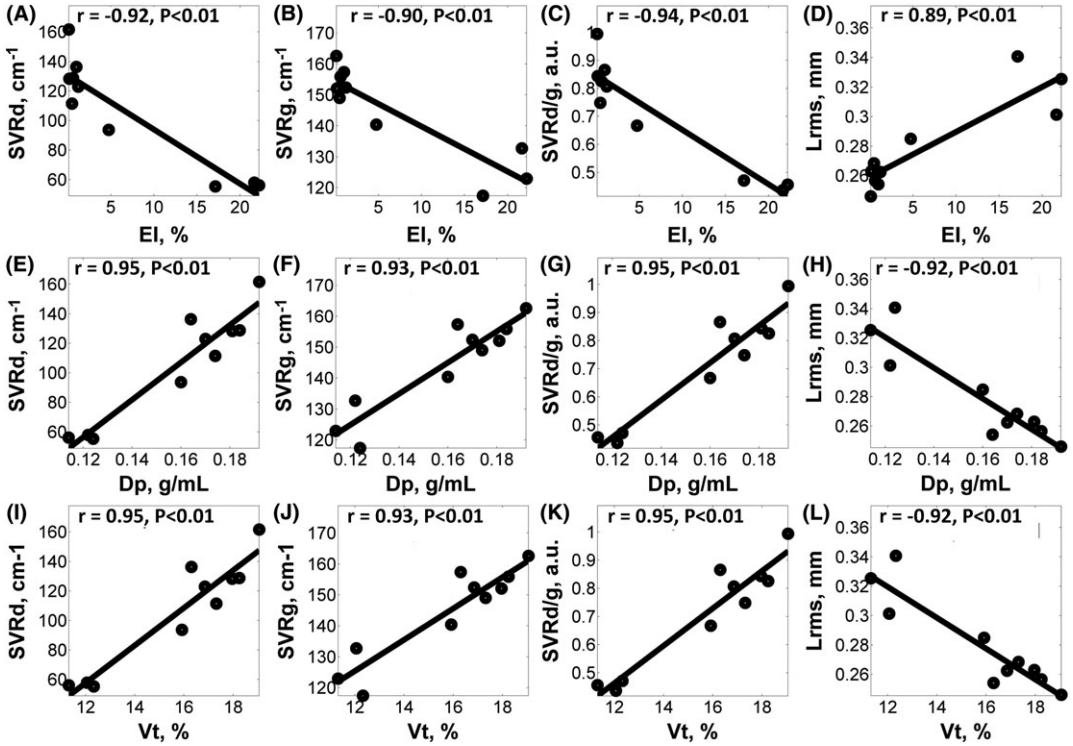

FIGURE 8 Comparison of SVR_d, SVR_g, $SVR_{d/g}$ and L_{rms} versus CT results (EI, D_p and V_t) in the AMC and COPD subjects. The SVR_d (A, E, I), SVR_g (B, F, J) and $SVR_{d/g}$ (C, G, K)) decreased as EI increased ($|r| > 0.89$, $P < 0.01$) and D_p and V_t decreased ($|r| > 0.92$, $P < 0.01$) while L_{rms} (D, H, L) correlated well with EI ($r = 0.893$, $P < 0.001$) and D_p ($r = -0.92$, $P < 0.001$) and V_t ($r = -0.919$, $P < 0.001$)

$SVR_{d/g}$ could be used to determine the extent of lung parenchyma destruction due to age and COPD. $SVR_{d/g}$ was intended to evaluate the surface of the pulmonary respiratory participating in blood-gas exchange normalized to an identical ventilation state, which is similar to the concept of the alveolar ventilation-perfusion ratio (V_A/Q).[36] There were no significant differences between AMC and COPD in TLC and FRC, and the influence caused by lung inflation level was reduced to consider the changes caused by pulmonary disease. The measured SVR_d, SVR_g, η, and $SVR_{d/g}$ values in the AMC subjects were much lower than that in the healthy young subjects. Meanwhile, the measured L_{rms} values were greater in AMC, which indicated that parenchyma changes and airspace enlargement coexisted as the age increased. Moreover, SVR_d, SVR_g, and $SVR_{d/g}$ correlated well with FEV_1(%pred) among the HY, AMC, and COPD subjects ($r > 0.86$, $P < 0.01$, Figure 6), which indicated that $SVR_{d/g}$ has potential in the evaluation of lung parenchyma changes caused by age. The measured SVR_d, SVR_g, and $SVR_{d/g}$ in the COPD subjects were much lower than those in the AMC subjects. Moreover, TP/gas and RBC/gas were lower in COPD than in AMC and HY ($P < 0.05$), but there was no significant difference in RBC/TP between AMC and COPD ($P = 0.315$). These results indicate the existence of destruction of the respiratory membrane as described in Reference 37. Meanwhile, the measured SVR_d, SVR_g, and $SVR_{d/g}$ decreased as EI increased ($|r| > 0.89$, $P < 0.001$) and D_p and V_t decreased ($|r| > 0.91$, $P < 0.001$), which indicated that less lung parenchyma participated in blood-gas exchange in COPD. Previous CT studies have demonstrated the process of narrowing and disappearance of small airways before the onset of emphysema in COPD subjects.[38] These results indicate the potential of $SVR_{d/g}$ in detecting the extent of lung parenchyma destruction caused by age and COPD in vivo. Because $SVR_{d/g}$ is sensitive to the changes of the pulmonary respiratory membrane, $SVR_{d/g}$ was expected to have an advantage over SVR_d and SVR_g in interstitial lung disease.[11]

$SVR_{d/g}$ was proposed to characterize the impairment of the respiratory membrane measured in the same breath-hold. SVR_d indicated the SVR of the pulmonary respiratory membrane participating in blood-gas exchange. SVR_g predicted the SVR associated with ventilation at specified size of the airspace. Because of the consistent gaseous xenon volume, $SVR_{d/g}$ could be used to evaluate the changes of the surface of the respiratory membrane normalized to the surface of the alveoli, which is hard to distinguish from the changes of thickness of the respiratory membrane in the traditional clinical examination. Therefore, simple airspace enlargement in the human lung could result in lower SVR_g and SVR_d while $SVR_{d/g}$ changes little. However, higher lung inflation level could result in much lower SVR_d[6,18,32] than expected, as the effective capillary capacity of the lung decreases. Besides, a previous study[32] has found a large coefficient of variation of SVR_d (14.1 ± 8.0% in healthy volunteers and 18.0 ± 19.3% in COPD patients) in short and long term reproducibility assessment. For the reproducibility of $SVR_{d/g}$, two aspects should be further investigated: (1) smaller number of delay times in CSSR to reduce the breath-hold time and (2) $SVR_{d/g}$ in the tidal volume of gas inhaled from FRC to assess the respiratory membrane in the daily lung inflation level.

Several limitations still existed in this study. First, the proposed method could only obtain the global pulmonary blood-gas exchange parameters, and dissolved xenon imaging technologies[12,37,39,40] should be combined with lung morphometric measurement and the advanced DWI

method[22] to comprehensively understand the microstructure and functions of the human lung using HP ^{129}Xe MR in the future. Second, the number of subjects was limited, and more healthy older subjects should be recruited to evaluate the changes in lung function and microstructure caused by age. Third, unlike the different lung inflation levels used in the studies of CSSR reproducibility,[32] only the lung inflation level of FRC + 1 L was used in this study, though no significant differences were found in the TLC and FRC between the AMC and COPD. Different lung inflation levels should be considered in further studies.

In conclusion, both gas-exchange and diffusion data were obtained within a single breath-hold to evaluate the respiratory membrane and pulmonary microstructure at identical inflation levels. Our results indicate that the proposed method has potential to detect the extent of lung parenchyma destruction caused by age and pulmonary diseases, and it would be useful in the early diagnosis of pulmonary diseases in clinical practice.

ACKNOWLEDGEMENTS

This work was supported by the National Natural Science Foundation of China (81625011, 81227902, 81601491), National Key R&D Program of China (2016YFC1304700 and 2017YFA0505400), the Key Research Program of Frontier Sciences, CAS (QYZDY-SSW-SLH018), and Hubei Provincial Natural Science Foundation of China (2017CFA013 and 2018ACA143). Xin Zhou acknowledges the support of the National Program for Support of Eminent Professionals (National Program for Support of Top-notch Young Professionals). We thank Dr Weiwei Ruan for his advice in data processing. The authors also thank David Donoho and Michael Lustig for sharing the original CS packages online.

ORCID

Xin Zhou https://orcid.org/0000-0002-5580-7907

REFERENCES

1. Albert MS, Cates GD, Driehuys B, et al. Biological magnetic resonance imaging using laser-polarized ^{129}Xe. *Nature*. 1994;370:199-201.
2. Ebert M, Grossmann T, Heil W, et al. Nuclear magnetic resonance imaging with hyperpolarized helium-3. *Lancet*. 1996;347:1297-1299.
3. Nikolaou P, Coffey AM, Walkup LL, et al. Near-unity nuclear polarization with an open-source ^{129}Xe hyperpolarizer for NMR and MRI. *Proc Natl Acad Sci U S A*. 2013;110:14150-14155.
4. Zhou X, Graziani D, Pines A. Hyperpolarized xenon NMR and MRI signal amplification by gas extraction. *Proc Natl Acad Sci U S A*. 2009;106:16903-16906.
5. Miller KW, Reo NV, Uiterkamp AJS, Stengle DP, Stengle TR, Williamson KL. Xenon NMR: chemical shifts of a general anesthetic in common solvents, proteins, and membranes. *Proc Natl Acad Sci U S A*. 1981;78:4946-4949.
6. Muradyan I, Butler JP, Dabaghyan M, et al. Single-breath xenon polarization transfer contrast (SB-XTC): implementation and initial results in healthy humans. *J Magn Reson Imaging*. 2013;37:457-470.
7. Månsson S, Wolber J, Driehuys B, Wollmer P, Golman K. Characterization of diffusing capacity and perfusion of the rat lung in a lipopolysaccaride disease model using hyperpolarized ^{129}Xe. *Magn Reson Med*. 2003;50:1170-1179.
8. Patz S, Muradian I, Hrovat M, et al. Diffusion of hyperpolarized ^{129}Xe in the lung: a simplified model of ^{129}Xe septal uptake and experimental results. *New J Phys*. 2011;13:015009.
9. Chang YV. MOXE: a model of gas exchange for hyperpolarized ^{129}Xe magnetic resonance of the lung. *Magn Reson Med*. 2013;69:884-890.
10. Matthew F, Alexei O, Elaine H, et al. Detection of radiation induced lung injury in rats using dynamic hyperpolarized ^{129}Xe magnetic resonance spectroscopy. *Med Phys*. 2014;41:072302.
11. Stewart NJ, Leung G, Norquay G, et al. Experimental validation of the hyperpolarized ^{129}Xe chemical shift saturation recovery technique in healthy volunteers and subjects with interstitial lung disease. *Magn Reson Med*. 2015;74:196-207.
12. Qing K, Mugler JP, Altes TA, et al. Assessment of lung function in asthma and COPD using hyperpolarized ^{129}Xe chemical shift saturation recovery spectroscopy and dissolved-phase MRI. *NMR Biomed*. 2014;27:1490-1501.
13. Li H, Zhang Z, Zhao X, Sun X, Ye C, Zhou X. Quantitative evaluation of radiation-induced lung injury with hyperpolarized xenon magnetic resonance. *Magn Reson Med*. 2016;76:408-416.
14. Saam BT, Yablonskiy DA, Kodibagkar VD, et al. MR imaging of diffusion of ^{3}He gas in healthy and diseased lungs. *Magn Reson Med*. 2000;44:174-179.
15. Kaushik SS, Cleveland ZI, Cofer GP, et al. Diffusion weighted hyperpolarized ^{129}Xe MRI in healthy volunteers and subjects with chronic obstructive pulmonary disease. *Magn Reson Med*. 2011;65:1155-1165.
16. Sukstanskii AL, Yablonskiy DA. Lung morphometry with hyperpolarized ^{129}Xe: theoretical background. *Magn Reson Med*. 2012;67:856-866.
17. Ouriadov A, Lessard E, Sheikh K, Parraga G. Pulmonary MRI morphometry modeling of airspace enlargement in chronic obstructive pulmonary disease and alpha-1 antitrypsin deficiency. *Magn Reson Med*. 2018;79:439-448.
18. Hajari AJ, Yablonskiy DA, Sukstanskii AL, Quirk JD, Conradi MS, Woods JC. Morphometric changes in the human pulmonary acinus during inflation. *J Appl Physiol*. 2012;112:937-943.
19. Patz S, Hersman FW, Muradian I, et al. Hyperpolarized ^{129}Xe MRI: a viable functional lung imaging modality. *Eur J Radiol*. 2007;64:335-344.
20. Lustig M, Donoho D, Pauly JM. Sparse MRI: the application of compressed sensing for rapid MR imaging. *Magn Reson Med*. 2007;58:1182-1195.

21. Ajraoui S, Parra-Robles J, Marshall H, Deppe MH, Clemence M, Wild JM. Acquisition of ^{3}He ventilation images, ADC, T_2^* and B_1 maps in a single scan with compressed sensing. *NMR Biomed*. 2012;25:44-51.
22. Abascal J, Desco M, Parra-Robles J. Incorporation of prior knowledge of signal behavior into the reconstruction to accelerate the acquisition of diffusion MRI data. *IEEE Trans Med Imaging*. 2018;37:547-556.
23. Chang YV, Quirk JD, Ruset IC, Atkinson JJ, Hersman FW, Woods JC. Quantification of human lung structure and physiology using hyperpolarized ^{129}Xe. *Magn Reson Med*. 2014;71:339-344.
24. Le Bihan D. Methods for MR measurement of diffusion In: Le Bihan D, ed. *Diffusion and Perfusion Magnetic Resonance Imaging: Applications to functional MRI*. New York: Raven; 1995:80-82.
25. Kärger J, Heink W. The propagator representation of molecular transport in microporous crystallites. *J Magn Reson*. 1983;51:1-7.
26. Lori NF, Conturo TE, Le Bihan D. Definition of displacement probability and diffusion time in *q*-space magnetic resonance measurements that use finite-duration diffusion-encoding gradients. *J Magn Reson*. 2003;165:185-195.
27. O'Halloran RL, Holmes JH, Wu YC, Alexander A, Fain SB. Helium-3 MR *q*-space imaging with radial acquisition and iterative highly constrained back-projection. *Magn Reson Med*. 2010;63:41-50.
28. Cambell H, Tomkeieff SI. Calculation of internal surface area. *Nature*. 1952;170:117.
29. Rabe KF, Hurd S, Anzueto A, et al. Global strategy for the diagnosis, management, and prevention of chronic obstructive pulmonary disease: GOLD executive summary. *Am J Resp Crit Care Med*. 2007;176:532-554.
30. Zhou X. Hyperpolarized noble gases as contrast agents. In: Schröder L, Faber C, eds. *In Vivo NMR Imaging*. New York: Humana; 2011:189-204.
31. Doel T. Pulmonary Toolkit. https://github.com/tomdoel/pulmonarytoolkit. Accessed May 23, 2015.
32. Stewart NJ, Horn FC, Norquay G, et al. Reproducibility of quantitative indices of lung function and microstructure from ^{129}Xe chemical shift saturation recovery (CSSR) MR spectroscopy. *Magn Reson Med*. 2017;77:2107-2113.
33. Paulin GA, Ouriadov A, Lessard E, Sheikh K, McCormack DG, Parraga G. Noninvasive quantification of alveolar morphometry in elderly never- and ex-smokers. *Physiol Rep*. 2015;3:e12583.
34. Weibel ER. *Morphometry of the Human Lung*. Berlin, Germany: Springer; 1963.
35. Thomen RP, Quirk JD, Roach D, et al. Direct comparison of ^{129}Xe diffusion measurements with quantitative histology in human lungs. *Magn Reson Med*. 2017;77:265-272.
36. Dantzker DR, Brook CJ, Dehart P, Lynch JP, Weg JG. Ventilation-perfusion distributions in the adult respiratory distress syndrome. *Am Rev Respir Dis*. 1979;120:1039-1052.
37. Kaushik SS, Robertson SH, Freeman MS, et al. Single-breath clinical imaging of hyperpolarized ^{129}Xe in the airspaces, barrier, and red blood cells using an interleaved 3D radial 1-point Dixon acquisition. *Magn Reson Med*. 2016;75:1434-1443.
38. McDonough JE, Yuan R, Suzuki M, et al. Small-airway obstruction and emphysema in chronic obstructive pulmonary disease. *N Engl J Med*. 2011;365:1567-1575.
39. Xie J, Li H, Zhang H, et al. Fast imaging of hyperpolarized Xe-129 in the airspace, barrier and red blood cells in the human lung. Proceedings of the 26th Annual Meeting of ISMRM, Paris, France, 2018. p 2440.
40. Ruppert K, Amzajerdian F, Hamedani H, et al. Rapid assessment of pulmonary gas transport with hyperpolarized ^{129}Xe MRI using a 3D radial double golden-means acquisition with variable flip angles. *Magn Reson Med*. 2018. https://doi.org/10.1002/mrm.27217

How to cite this article: Xie J, Li H, Zhang H, et al. Single breath-hold measurement of pulmonary gas exchange and diffusion in humans with hyperpolarized ^{129}Xe MR. *NMR in Biomedicine*. 2019;e4068. https://doi.org/10.1002/nbm.4068